The Statistics of Vestibular Recalibration

Master's Thesis

Cleo Ariata

Delft University of Technology

TU Delft

The Statistics of Vestibular Recalibration

Master's Thesis

by

Cleo Ariata

Student number: 5297923

to obtain the degree of Master of Science in Biomedical Engineering, track Medical Devices
at the Delft University of Technology,
to be defended publicly on Tuesday December 9, 2025 at 9:30 AM.

Committee chair:	Prof.dr.ir. Alfred.C Schouten
Committee members:	Dr. Patrick Forbes, Dr. Dimitra Dodou
Degree:	Biomedical Engineering MSc
Faculty:	Faculty of Mechanical Engineering, Delft

TU Delft

Acknowledgments

I would first like to express my sincere gratitude to dr. Patrick Forbes for his continuous support, guidance, and encouragement throughout the entirety of this project. His day-to-day involvement and willingness to help at every stage were extremely valuable. I would also like to thank prof.dr.ir Alfred Schouten for his insightful feedback and for providing direction whenever needed. I am grateful to Erasmus MC for kindly allowing me to conduct my experiments within their facilities and for providing an environment that made this work possible. Finally, I would like to thank my friends and family for their support, patience, and belief in me throughout this journey.

Abstract

The vestibular system plays a central role in maintaining upright balance by encoding head motion and integrating this information with visual and somatosensory cues. When the relationship between self-motion and vestibular input becomes unreliable, the central nervous system (CNS) adapts to preserve postural stability. Previous studies demonstrated that adaptation occurs when altered vestibular input remains coherently linked to head movement; however, it remains unclear whether recalibration persists when this motion–afference relationship is degraded by non-coherent noise (Héroux et al. (2015); Chen et al. (2020)).

This report investigates vestibular recalibration under two forms of galvanic vestibular stimulation: a coherent, head-coupled stimulus derived from a validated motion-to-current conversion model, and the same stimulus combined with high-amplitude non-coherent noise. Fourteen participants completed standing-balance trials assessing baseline sway, externally replayed vestibular perturbations, and short-term learning during a brief eyes-open calibration period. Postural stability was quantified using T1 lateral displacement, and adaptation was assessed by comparing sway variability before and after calibration.

Under coherent stimulation, participants exhibited clear recalibration: sway variability increased immediately after stimulation onset but decreased during calibration, returning toward baseline levels. In contrast, non-coherent stimulation produced substantially greater sway and reduced adaptive improvement, indicating that noise limits the CNS's ability to reinterpret vestibular input. Nonetheless, some recalibration was still observed, although highly variable across individuals. Additional findings revealed transient post-stimulation after-effects and modest order-dependent influences, though these did not reach statistical significance.

Overall, the results indicate that vestibular recalibration depends critically on the coherence and reliability of motion-linked vestibular input. When the motion–afference mapping is degraded by an external noise source, the CNS down-weights vestibular cues and exhibits limited adaptive learning.

Contents

1

Introduction

Upright balance depends on the integration of sensory information originating from somatosensory, visual, and vestibular systems. The vestibular system contributes critically to this process by encoding head motion and spatial orientation through the semicircular canals and otolith organs. These sensory cues support stable perception and coordinated motor output during everyday movement. An essential characteristic of motor behavior is sensorimotor recalibration, in which internal predictions are continuously updated to align expected and actual sensory consequences of movement (Shadmehr et al. (2008)). This recalibration process relies on comparing predicted sensory consequences, derived from motor commands, with the actual sensory feedback. When this relationship changes—for example, when visual cues become noisy or unstable, such as during fog or rapid head movements—the nervous system must reinterpret these inputs to maintain effective motor control. Such changes can arise from many sources, including environmental disturbances or altered sensorimotor mappings.

A key component of this recalibration process is the ability to integrate and reweight multisensory information. When one sensory channel becomes unreliable, its contribution to postural control is down weighted in favor of more reliable cues (Carriot et al. (2015)). Vision is typically the most precise source of spatial information, and access to visual cues therefore enables the nervous system to reestablish a coherent estimate of body motion and orientation. Reopening the eyes following vestibular perturbation increases reliance on vision and proprioception, allowing recovery of postural stability despite degraded vestibular input (Fitzpatrick and Day (2004); Maurer et al. (2005)). This reweighting mechanism provides a physiological basis for why visual exposure can function as a "calibration" phase.

Previous work has shown that the nervous system can recalibrate its estimates of self-motion when the vestibular signal of head motion is artificially distorted. Héroux et al. (2015) reported that real-time, head-coupled galvanic vestibular stimulation (GVS) initially destabilized balance in the absence of vision, as the altered mapping between head motion and vestibular sensation introduced a sensory–motor conflict. After a conditioning period with reliable visual or somatosensory cues, postural stability returned despite continued stimulation, indicating that the altered vestibular input was reinterpreted as self-generated. More recently, Chen et al. (2020) described a physiological model, based on Héroux et al. (2015), that transforms measured head motion into equivalent electrical vestibular stimulation, enabling more realistic manipulation of vestibular afference. Collectively, these studies showed that the nervous system can adjust when the correspondence between motion and vestibular sensation is systematically modified, provided the distorted signal is coupled to ongoing head motion.

While adaptation is observed when the altered vestibular signal retains coherence with self-motion, it

is unclear whether similar recalibration occurs when that relationship is degraded by introducing substantial noise. This motivates the central research question of this thesis: *Is the nervous system able to recalibrate its expectation of motion when the inherent motion-to-sensation relation is compromised by noise?* The present work addresses this question using a closed-loop GVS structure based on the conversion model developed by Chen et al. (2020). Participants experienced vestibular stimulation that was either coherently linked to head motion or combined with high-amplitude non-coherent noise. The hypothesis proposes that coherent stimulation facilitates recalibration and the restoration of stable balance following conditioning, whereas non-coherent noise that disrupts the motion-dependent mapping is expected to attenuate recalibration and impede postural recovery.

2

Materials and Methods

2.1. Subjects

Fourteen participants (5 female; age range: 21–56 yr) completed the experimental protocol. All participants reported no prior neurological disorders, injuries, or balance impairments before enrollment. Participants received information about the procedures and potential discomforts and were free to discontinue participation at any time. Written informed consent was obtained prior to testing. All procedures adhered to the Declaration of Helsinki (2024) and complied with the Medical Research Involving Human Subjects Act (WMO).

2.2. Experimental setup

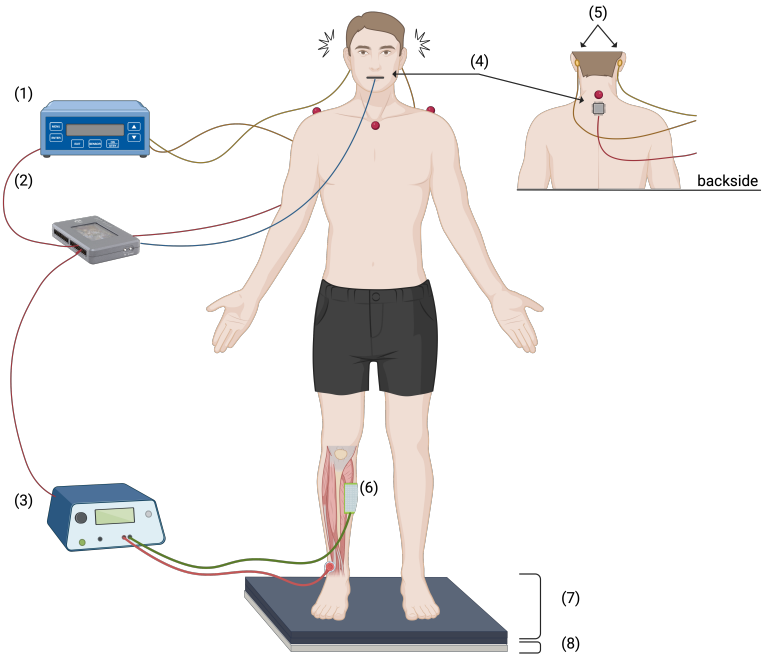

Figure 2.1: Experimental setup
(1) Stimulator, (2) myRIO, (3) EMG Amplifier, (4) Inertial Measurement Units, (5) Rubber electrodes, (6) EMG High Density Grid, (7) Foam mat (8) Force plate
This figure was created in BioRender. Ariata, C. (2025) https://BioRender.com/sdxjzwg

The experimental setup included a BP400600-OP force plate for measuring ground-reaction forces, an 8-camera motion-capture system for recording body kinematics, and a custom mouthguard-mounted IMU for measuring head motion. Vestibular stimulation was delivered using a bipolar binaural electrode

configuration connected to an isolated constant-current stimulator controlled by an NI myRIO-1900. Surface EMG of the medial gastrocnemius was recorded using a surface high-density electrode grid and was amplified using an EEG amplifier (Refa Ext-128e4b4a). An overview of the setup is shown in Figure 2.1. Further details on the purpose, implementation, and calibration of each component are provided in the subsequent sections.

2.3. Electrical Vestibular Stimulation model

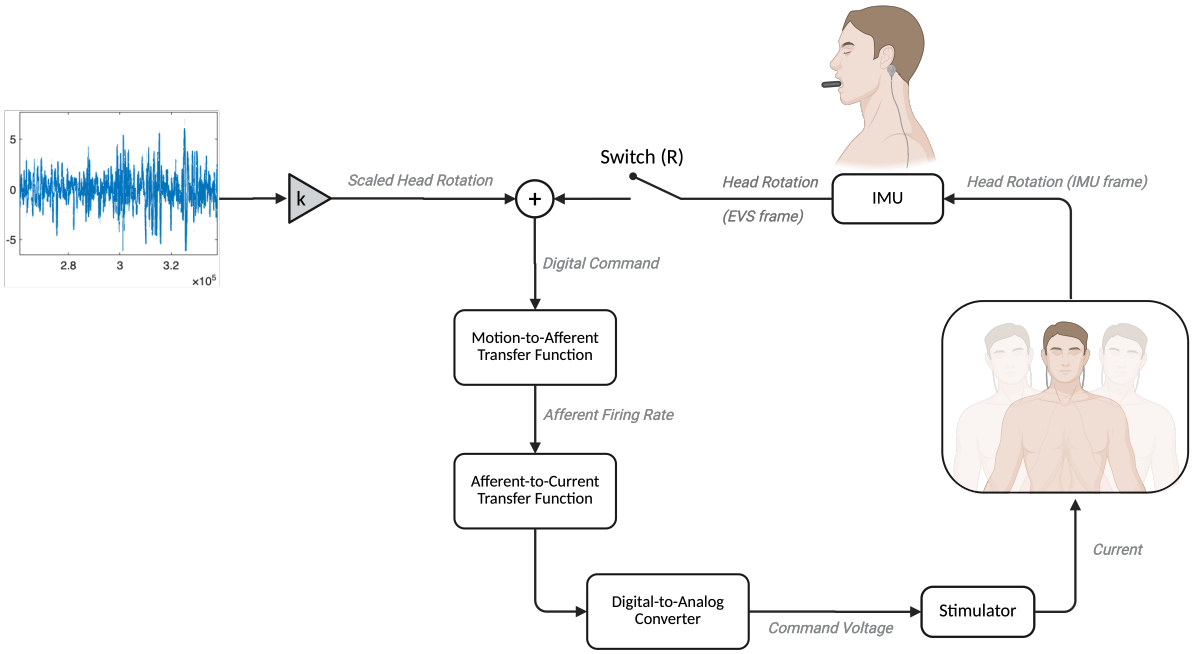

Figure 2.2: Model of vestibular sensory control for balance
k: external stimulus scale factor, R: real-time stimulation on and off switch
This figure was created in BioRender. Ariata, C. (2025) https://BioRender.com/91h9m57

The aim of the stimulation model used in this study is to convert measured head angular velocity into a transmastoid electrical current that evokes vestibular afferent activity equivalent to that produced by natural head motion. This follows the approach introduced by Chen et al. (2022), who developed a real-time mapping by combining three experimentally derived relationships: (1) how vestibular afferents encode natural mechanical rotation, (2) how they respond to galvanic stimulation, and (3) how to invert the galvanic response so that a desired afferent pattern can be generated electrically. The resulting model enables controlled manipulation of the motion–to–afferent relationship during standing balance, and the following sections summarise the essential contributions of the models by Schneider et al. (2015); Kwan et al. (2019) and Chen et al. (2020).

2.3.1. Motion to Afferent Model

Schneider et al. (2015) provided a quantitative description of how regular and irregular semicircular canal afferents encode angular head velocity across frequencies. Using sinusoidal mechanical rotations in macaques, they fitted afferent firing rates with a sinusoidal model,

$$FR(t) = \text{gain} \cdot \text{stimulus}(t + \theta) + \text{bias},$$

to obtain frequency-dependent gain and phase. Population-averaged data were then represented using a linear transfer function in the Laplace domain. For canal afferents, the best-fit model (their Eq. 1) took

the form

$$H_{\text{canal}}(s) = \frac{h\,s(s + 1/T_1)(s + 1/T_c)}{(s + 1/T_2)},$$

where h is the overall sensitivity, T_1 and T_2 capture high-frequency dynamics, and T_c represents the dominant cupula time constant. The experimentally derived parameter values used in this study are:

- Regular afferents: $h = 2.83$, $T_1 = 0.0175\,\text{s}$, $T_2 = 0.0027\,\text{s}$, $T_c = 5.7\,\text{s}$
- Irregular afferents: $h = 27.09$, $T_1 = 0.03\,\text{s}$, $T_2 = 0.0006\,\text{s}$, $T_c = 5.7\,\text{s}$

These transfer functions capture the essential frequency-dependent differences between afferent classes: irregular afferents show higher gain and faster dynamics, whereas regular afferents encode a smoother, lower-gain representation of motion. In the present study, the motion–to–afferent relationship described by Schneider et al. (2015) is implemented using separate transfer functions for regular and irregular afferents. These are later incorporated into the full conversion model (see Section 2.3.3). We denote these functions as

$$H_{\text{MO,reg}}(s), \quad H_{\text{MO,irreg}}(s).$$

2.3.2. Electrical Current to Afferent Model

Kwan et al. (2019) extended Schneider's methodology to GVS, characterising how the same afferents respond to electrical currents instead of mechanical rotation. Using sinusoidal transmastoid currents (0.1–25 Hz) in behaving monkeys, they found that afferents again exhibited frequency-dependent gain and phase behavior that could be described using transfer functions. Their population fits were expressed as

$$FR(t) = \text{gain} \cdot GVS(t + \theta) + \text{bias},$$

leading to a transfer-function representation of the form

$$H(s) = h\,\frac{(s + b_1)(s + b_2)}{(s + a_1)(s + a_2)}, \tag{2.1}$$

parameterised separately for regular and irregular afferents.

In the present work, these current–to–afferent transfer functions are used in their inverted form so that a desired afferent response can be mapped back to an equivalent electrical current. The inverted functions used here are (after Chen's implementation):

$$H_{E_{\text{reg}}}(s) = \text{inv}\left(\frac{98(s + 26)(s + 188)}{(s + 47)(s + 2578)}\right) \cdot 0.75$$

$$H_{E_{\text{ireg}}}(s) = \text{inv}\left(\frac{418(s + 12)(s + 136)}{(s + 18)(s + 2739)}\right) \cdot 0.25$$

These describe the electrical input required to obtain a specific afferent firing pattern.

2.3.3. Motion to Electrical Stimulation Model

Chen et al. (2022) combined Schneider's motion–to–afferent model and the inverted Kwan afferent–to–current model to produce a real-time mapping that converts measured head motion into an equivalent electrical stimulus. The model is constructed by cascading the two stages:

$$\text{Head Motion} \xrightarrow{\boxed{H_{\text{MO}}(s)}} \text{Afferent Firing} \xrightarrow{\boxed{H_{\text{E}}^{-1}(s)}} \text{Electrical Current.}$$

To capture the combined contribution of regular and irregular vestibular afferents, the motion–to–afferent stage is expressed as a weighted sum of the two pathways. Following Chen et al. (2022), the regular pathway contributes with weight 0.75, and the irregular pathway with weight 0.25, reflecting their approximate physiological proportions.

Using this weighted combination for the motion–to–afferent stage, its cascade with the afferent–to–current model produces the complete motion–to–current conversion:

$$I(s) = G\left[H_{\mathrm{MO,reg}}(s) + H_{\mathrm{MO,irreg}}(s)\right]\left[H_{\mathrm{E,reg}}(s) + H_{\mathrm{E,irreg}}(s)\right],$$

corresponding to Eq. (5) in Chen et al. (2022). A scalar gain $G = 4.23$ ($0.37\ \mathrm{mA{\cdot}deg^{-1}s}$) sets the overall conversion factor so that the resulting current produces afferent activation equivalent to natural head rotation in humans.

For real-time stimulation, these continuous transfer functions are discretised and implemented on the myRIO controller. Instantaneous head angular velocity is fed into the digital model to compute the GVS current with minimal delay. This ensures that stimulation remains tightly coupled to head movement during the experiment, while allowing additional non-coherent noise to be added when required by the experimental condition.

2.4. Vestibular Stimulation

Galvanic vestibular stimulation is used to alter vestibular input in a controlled, movement-dependent manner. Carbon–rubber electrodes coated with conductive gel are positioned over the mastoid processes to deliver current using a bipolar–binaural configuration, which modulates afferent activity along the net GVS-evoked rotational vector (Khosravi Hashemi et al. (2019)).

Stimulation is generated using an isolated constant-current stimulator (maximum output ± 10 mA), limited in practice to ± 6 mA by software and hardware constraints. The current signal is delivered through a National Instruments data-acquisition board interfaced with a myRIO-1900 microcontroller. Delivering current in constant-current mode ensures that injected current amplitude remains stable despite variations in skin–electrode impedance (Chen et al. (2022)).

The stimulation signal is derived from real-time measurements of head angular velocity. In the main experimental condition, this velocity is converted to an equivalent current using the transfer-function model described in Section 2.3. By coupling the primary stimulation to instantaneous head motion, vestibular perturbations are restricted to periods of movement. Controlled degradation of the motion-to-sensation mapping is introduced by adding a secondary, non–head-coupled noise signal to the motion-dependent input (Chen et al. (2022)).

2.5. Kinematic Motion Capture

The kinematic behavior of specific body segments is recorded using markers placed on the sternum, T1 vertebra, and bilateral acromia. Marker positions are measured using an 8-camera motion-capture system, which enables reconstruction of body posture and sway patterns across stimulation conditions. Quantifying postural behavior provides an independent assessment of how altered vestibular afference affects balance control (Héroux et al. (2015)).

2.6. Mouthguard and Head-Motion Sensing

Accurate measurement of head motion is critical for generating the velocity-coupled GVS signal. An inertial measurement unit (IMU; MPU-6000) is therefore mounted on a custom mouthguard. Because the maxilla is rigidly coupled to the skull, this placement minimizes soft-tissue artefacts (Wu et al. (2015)). It further reduces activation of muscles adjacent to the mastoid region, thereby preventing jaw

clenching or biting from perturbing the stimulation through changes in electrode contact or impedance. Head angular velocity is measured continuously and transformed into the GVS reference frame using participant-specific calibration procedures (Section 2.7).

2.7. Coordinate Frame Calibration

To align the IMU recordings with the predicted GVS rotational axis, each participant completed two static calibration trials: a face-forward pose with the head pitched approximately 18° above Earth-horizontal, and a face-down pose with Reid's plane tilted 18° past vertical. Reid's plane, defined by the inferior orbital rim and the external auditory meatus, was oriented to these two positions using a protractor and level. These known head orientations allow us to determine how the IMU axes align with gravity. By comparing the measured acceleration vectors with the expected gravitational directions in each pose, we compute a transformation matrix that rotates the raw IMU coordinate frame into the GVS reference frame. Three-dimensional acceleration data were collected for 10 seconds in each pose to construct this transformation, ensuring that the resulting angular velocity measurements align with the physiologically relevant GVS rotational axis. For details regarding the implementation of these transformations please see Chen et al. (2022).

2.8. Experimental Protocol

Each participant completed seven standing-balance trials on a foam pad. Handrails were positioned on both sides to ensure participant safety; however, their presence restricted lateral movement to an area of approximately 1 m × 1 m. To minimize the effect of this constraint, participants were instructed to use the handrails only if necessary to prevent a fall. A researcher was present throughout the experiment to provide additional supervision and reassurance.

The first trial, *Natural standing balance*, required participants to stand upright with eyes closed for 120 s without electrical vestibular stimulation. This was followed by four *Vestibular variability* trials (60 s each), conducted under identical conditions except that participants received externally generated vestibular stimulation scaled by factors between 1 and 4. The external stimulation was produced by processing the head-motion signal recorded during the natural standing balance trial using the transfer functions described previously, and replaying the resulting signal to the participant. No real-time velocity coupling was implemented during these trials.

The final two trials constituted the *Main* experimental protocol, as seen in Figure 2.3. In these trials, participants received a combination of real-time head-motion-coupled stimulation and scaled external stimulation. Each trial consisted of the following phases:

- Baseline (40 s): Eyes closed; no GVS.
- Pre-conditioning (60 s): Eyes closed; GVS active and coupled to head-roll motion.
- Conditioning (180 s): Eyes open; participants performed natural head movements while GVS remained active.
- Post-conditioning (60 s): Eyes closed; GVS active and coupled to head-roll motion.
- Recovery (60 s): Eyes closed; no GVS.

Participants were randomly assigned to one of two order groups. Group A experienced the no-noise condition first, followed by the noise condition. Group B experienced the noise condition first, followed by the no-noise condition. This grouping enabled counterbalancing of potential order effects and allowed evaluation of whether exposure order influenced recalibration or postural variability.

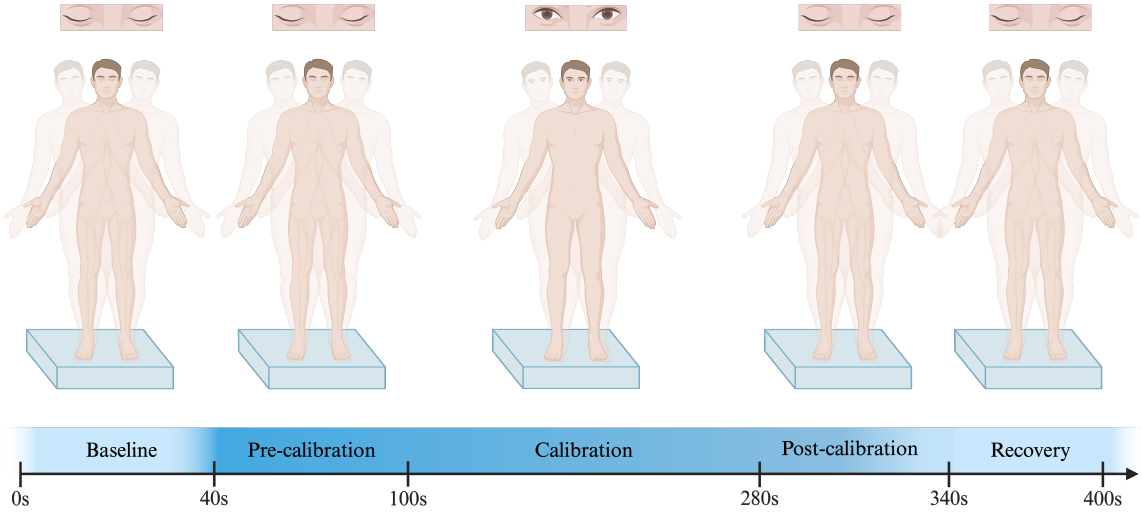

Figure 2.3: Experimental protocol timeline.
Created in BioRender. Ariata, C. (2025) https://BioRender.com/wjowm09

2.9. Data & Signal Processing

2.9.1. Instrumentation and Acquisition

Stimulation delivery and inertial data collection were implemented using LabVIEW. Motion-capture data were collected in parallel using Qualisys Track Manager (QTM, Qualisys AB, Sweden), providing whole-body kinematics during each trial. Body motion was quantified via an MPU-6000 IMU, which records tri-axial linear acceleration and angular velocity. The accelerometer sensitivity was set to ±2 g, and the gyroscope to ±250°/s, the lowest selectable ranges for this device. These settings are chosen to maximize measurement resolution while still accommodating the expected dynamic range of human standing balance. The sampling rate for both real-time stimulation and calibration procedures is fixed at 100 Hz. Operation at 100 Hz yielded minimal latency loops and results in an estimated system delay of approximately 10 ms. However, the IMU sensor itself does not contribute to any additional delay.

A myRIO-1900 microcontroller serves as the interface between the IMU, host computer, and stimulation circuitry. The unit was mounted to a custom fabricated electrical board designed to standardize signal routing and minimize wiring complexity and an inline hardware filter was incorporated on this board.

2.9.2. System Synchronization

All recording devices were temporally synchronized via a trigger signal generated by the myRIO and distributed to all systems. Upon operator initiation, this trigger concurrently started QTM motion-capture recording, initiated GVS stimulus generation in LabVIEW, and recorded stimulus onset timestamps in both QTM and the EMG acquisition system.

LabVIEW data recording was initiated slightly earlier to ensure a complete 40s measurement window that encompasses the stimulus period. This synchronization procedure enabled precise temporal alignment across all hardware systems, simplifying both real-time monitoring and post-processing analysis.

For subsequent analysis, the primary parameter extracted from QTM was the displacement of the T1 marker along the right–left (y) axis, representing overall postural sway. Additional analyses incorporated head motion around the roll (x) axis, obtained directly from the inertial measurement unit (IMU).

2.9.3. LabVIEW Data Handling

During acquisition, IMU data were read in real time using a custom LabVIEW VI. The output from all sensors was compiled into a single data structure containing:

- time stamps,
- trigger signal,
- IMU data calibrated to the GVS reference frame,
- weighted total stimulus,
- weighted real-time stimulus,
- weighted external stimulus,
- external stimulus scaling factor (k), and
- real-time switch parameter (R).

The head-motion signal, expressed as current per angular velocity ($\mathrm{mA \cdot deg^{-1} \cdot s}$), was multiplied by the instantaneous head velocity recorded by the IMU. The resulting real-time stimulus (RT stim) was then scaled by the parameter R to obtain the weighted RT stimulus. Similarly, the external stimulus was multiplied by k to compute its weighted value before being transmitted to the stimulator.

2.9.4. Motion Capture

Following data collection, motion-capture markers were manually labeled in QTM. The T1 marker trajectory was extracted for analysis. Any missing data points were interpolated using QTM's built-in polynomial gap-filling function. The processed motion data were then exported and organized in MATLAB for each participant and trial, including information on condition, trial duration, T1 position, trigger timing, and recorded stimulation signals.

Data Processing in MATLAB

All datasets were organized into participant-specific MATLAB structures. Data were segmented to remove samples recorded before the trial trigger and, where applicable, after the stimulus offset. To reduce high-frequency sensor noise, a fourth-order Butterworth low-pass filter with a 10 Hz cutoff frequency was applied, consistent with pilot analyses indicating that postural sway occurs below this range.

After filtering, the head-motion signal, stimulus signals, and T1 displacement were each divided into five temporal segments corresponding to the predefined phases of the main trials. This segmentation enabled direct comparison across experimental steps and conditions. All subsequent analyses were performed in MATLAB (MathWorks, Natick, MA, USA).

2.9.5. Outcome Measures

The primary metric used to assess changes in postural stability across conditions was the standard deviation (SD) of the displacement of the T1 along the right–left (y) axis. This metric served as the primary input for the outcome measures detailed in this section. To quantify improvement following the calibration phase, the *learning* parameter was used. It is defined as:

$$\text{Learning} = \frac{\mathrm{SD_{pre}} - \mathrm{SD_{post}}}{\mathrm{SD_{pre}}},$$

where $\mathrm{SD_{pre}}$ and $\mathrm{SD_{post}}$ represent the standard deviation of T1 displacement measured before and after calibration, respectively. A positive value of the learning parameter indicates a reduction in sway

variability following calibration, reflecting improved postural control.

To gauge whether any stimulation effect persists after it is turned off, we compute the after-effect as

$$\text{After-effect} = \text{SD}_{\text{Recovery}} - \text{SD}_{\text{Baseline}},$$

A positive after-effect indicates that variability during the recovery period remains elevated relative to baseline, suggesting the effect has not fully dissipated. A negative value indicates that recovery variability has returned to, or fallen below, baseline levels.

In addition, a relative standard deviation (*relative SD*) was computed to compare pre-calibration sway variability to baseline performance:

$$\text{Relative SD} = \frac{\text{SD}_{\text{pre}} - \text{SD}_{\text{baseline}}}{\text{SD}_{\text{baseline}}}.$$

This parameter normalizes pre-calibration variability against the participant's baseline sway, allowing comparison across individuals and conditions. Together, these measures provide quantitative indices of postural adaptation and recalibration.

The computed learning and relative SD parameters were then used to evaluate postural adaptation across participants and conditions. For each trial, these measures were averaged across the five temporal segments defined in the experimental protocol. Statistical analyses compared values obtained before and after calibration, as well as across different stimulation conditions, to determine whether exposure to coherent or noisy vestibular input influenced the recalibration of balance control. The resulting group means and individual data are presented in the following section.

For specific analyses, the overall standard deviation was insufficient to capture the temporal dynamics of postural control. To characterize how sway variability evolved throughout the trial, a *sliding standard deviation* was computed, allowing moment-to-moment changes in stability to be identified. This approach detects transient increases or decreases in sway that would be obscured by a single value averaged over the entire 40-s recovery period. Variability was calculated using a 5-s sliding window with a 1-s step size for each group and condition.

Statistical Analysis

All statistical analyses were conducted in MATLAB or JASP. Statistical significance was set at $p < 0.05$ and marginal effects ($0.05 \leq p < 0.10$) were treated as non-significant trends.

A two-way mixed ANOVA was used to evaluate effects of Condition (no-noise, noise; within-subject) and Order (Group A: no-noise→noise, Group B: noise→no-noise; between-subject) on absolute and baseline-normalized SD. Deviations from homogeneity were assessed using Levene's test. For the vestibular variability trials, Levene's test was additionally used to examine scaling-dependent changes in between-subject variability.

Learning effects were compared between stimulation conditions using an independent-samples Welch's t-test, restricted to trials in which each condition was experienced first to avoid carryover effects. Relationships between natural postural stability and learning were assessed via Pearson correlations between baseline SD and learning index.

To assess post-stimulation after-effects, paired t-tests compared baseline SD with recovery SD within each order group. Temporal evolution of postural variability during recovery was examined using a 5-s sliding-window SD, providing a high-resolution estimate of post-stimulus decay.

3

Results

3.1. Vestibular Variability

In this study, participants first performed vestibular variability trials where they were exposed to an external stimulus that was based upon their own baseline motion trial (Figure 3.1). Each trial corresponded to an increasing level of externally generated vestibular stimulation. Because the external stimulus, in these trials, was obtained by replaying the participant's own baseline motion with scaling factors between 1 and 4, higher scaling factors effectively introduced stronger vestibular perturbations. This relationship appeared approximately linear, indicating that postural instability scaled proportionally with the magnitude of the imposed vestibular disturbance.

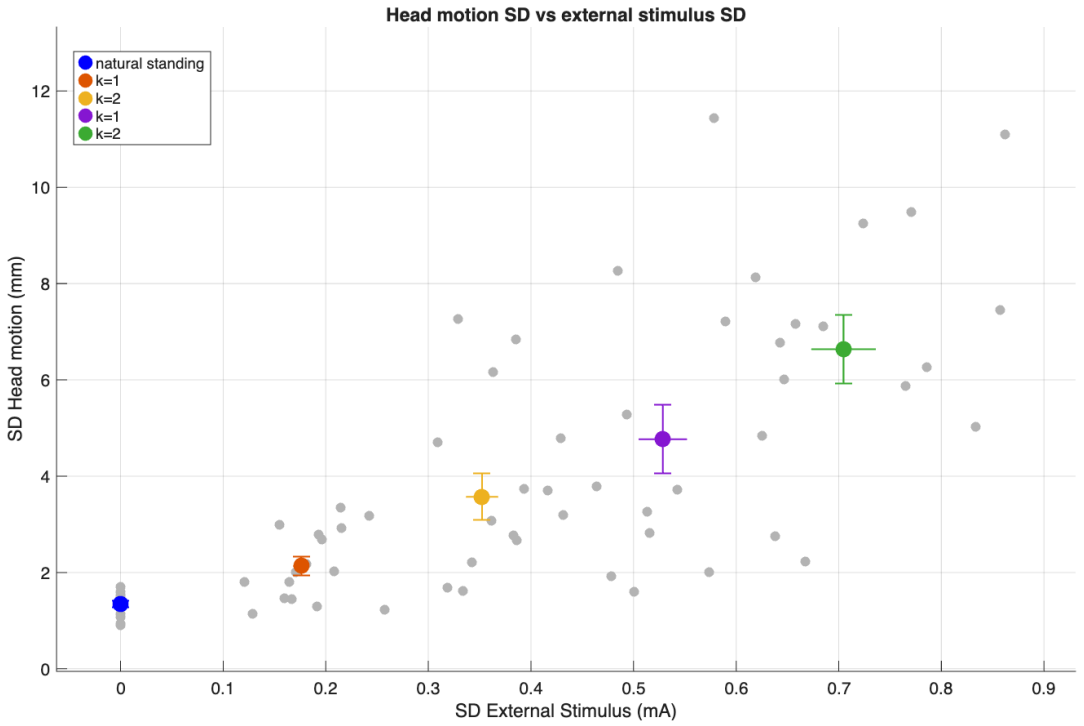

Figure 3.1: Standard deviation of head lateral displacement across the baseline and four vestibular variability trials. Increasing the external stimulus amplitude resulted in a proportional increase in sway variability, indicating that stronger externally generated vestibular input induces greater postural instability. Each point represents an individual participant. The coloured circular markers represent the different conditions: blue indicates natural standing, while red, yellow, purple, and green correspond to increasing levels of external stimulus (k), as shown in the legend. Error bars indicate the group mean ± SEM.

All variability trials were conducted with eyes closed and without real-time coupling, which implies that the external stimulation had no causal relationship to the participant's current head motion. Consistent with expectations, when vestibular afference was decoupled from natural movement, the nervous system was less able to suppress or reinterpret the perturbation, consistent with increased sway variability. These findings confirmed that participants were sensitive to the amplitude of vestibular noise and that the induced variability provided a reliable reference point for interpreting adaptation behaviour in the main experiment.

Additional observations further clarified this relationship. Inter-individual variability increased with higher stimulus scaling, suggesting that some participants were more susceptible to externally generated vestibular noise than others. This observation was confirmed statistically: Levene's test showed a significant difference in variance across scaling levels ($p = 0.00053$), indicating that between-subject variability reliably increased as stimulus intensity rose. Moreover, the approximately linear trend across scaling factors suggests that the perturbation acted primarily as additive vestibular noise rather than producing nonlinear or threshold-like destabilization effects.

3.2. Learning Under Coherent GVS Stimulation

In the main trials, a consistent pattern of postural variability emerged across participants for the conditions experienced first. During the baseline phase, participants displayed natural quiet-standing sway. In the pre-calibration phase, the introduction of vestibular stimulation produced a pronounced increase in sway variability. This variability decreased during the post-calibration phase, indicating partial recalibration of the vestibular input when visual cues were available. In the subsequent no-GVS recovery phase, sway variability returned toward baseline levels, although it remained slightly elevated.
Participants experiencing the coherent condition second had the overall sequence of variability changes that followed a similar structure; however, a key deviation emerged: sway variability increased from the pre-calibration to the post-calibration phase. This pattern suggests the presence of a lingering aftereffect from the first trial, influencing participants' responses in the second trial. This phenomenon is examined further in Section 3.5.

A one-sample t-test showed that participants in the coherent-first condition showed a trend toward improved sway variability (mean learning 18.7%, $p = 0.086$), as seen in Figure 3.2(A). Although this did not reach significance, the predominantly positive learning values suggest some degree of recalibration in most participants. The lack of statistical significance may reflect the small sample size and substantial inter-individual variability, rather than the absence of a true effect. This recovery, from pre calibration to post calibration, is consistent with the idea that when vestibular input remains causally tied to self-motion, the central nervous system can reinterpret the altered signal as self-generated and adjust its internal model accordingly.

3.3. Learning Under Non-Coherent GVS Stimulation

A key question in this experiment is whether adding a non-coherent (noise) stimulus to the real-time correlated vestibular signal affects participants' ability to adapt after a short recalibration period. As shown in Figure 3.2B, participants exposed to non-coherent stimulation in addition to the coherent input, had postural responses that followed a progression across phases similar to that observed in the coherent condition, both when the condition was experienced first and when it was experienced second. However, for trials experienced first, sway variability during the pre- and post-calibration phases was substantially higher than in the coherent condition. On the other hand, participants in the noise condition exhibited a smaller relative improvement in postural stability following calibration (12.87%) compared to those in the no-noise condition. This pattern suggests that the presence of noise may hinder short-term vestibular recalibration.

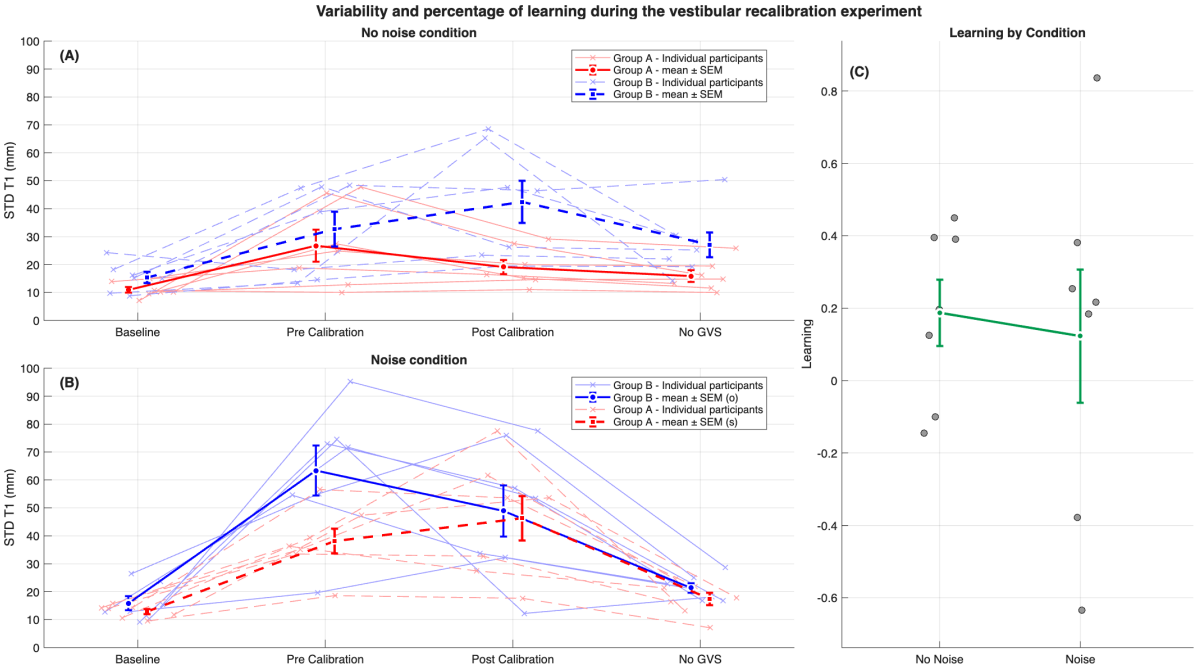

Figure 3.2: (A) The standard deviation of T1 displacement along the medio-lateral axis is shown for four experimental segments corresponding to different phases of the vestibular recalibration task: Baseline, Pre-Calibration, Post-Calibration, and Recovery. Each colored "×" represents an individual participant, while the bold markers with error bars indicate the group mean ± SEM. Red lines and symbols correspond to Group A, and blue lines and symbols correspond to Group B. Solid lines indicate data from the condition when it was experienced first in the experiment, whereas dashed lines indicate data from the condition when it was experienced second. (B) Same metrics as in (A), but for trials with the Noise condition instead of the No-Noise condition. (C) Percentage learning for each participant computed within the condition they experienced first (No-Noise or Noise) and reflects the relative change in sway variability from the Pre-Calibration to the Post-Calibration segment.

This reduction in learning is also visible in Figure 3.2C, where only the trials in which each condition was experienced first were compared, removing potential order effects. Overall postural variability is consistently higher in the noise condition than in the no-noise condition, in line with the idea that non-coherent stimulation disrupts balance and increases sway. However, statistical testing does not support a reliable difference between conditions. An independent-samples Welch's t-test on percentage learning values shows mean learning of 0.19 (SD = ±0.24) in the no-noise condition and 0.12 (SD = ±0.49) in the noise condition. The difference is not statistically significant ($p = 0.76$).

Although the mean learning was numerically lower in the noise condition, the difference was not statistically significant, and the wide confidence intervals mean the data is inconclusive regarding any true difference in learning between conditions. The absence of a strong difference suggests that participants may still be able to use the coherent component of the signal for recalibration, even when non-coherent noise is present.

3.4. Comparison of Post Calibration Responses with Baseline and Vestibular Variability Trials

A comparison between the standard deviation of T1 displacement during the post-calibration segment of the main trials and the corresponding vestibular variability trials provides insight into the extent of adaptation to real-time stimulation. If participants fully adapt to the RT stimulus, the post-calibration variability is expected to approximate the variability induced by the external stimulus. Postural variability after calibration also returned toward values comparable to baseline standing, although the extent of this recovery depended strongly on the stimulation condition and the order in which it was experienced.

In the noise condition, this pattern is clearly present: both group A and group B showed post-calibration standard deviations that closely matched the vestibular variability values (group B: 48.9 mm; group A: 46.3 mm; vestibular variability: 47.82 mm). When the high-noise condition was experienced first, this same pattern was observed at the group level (mean = 48.91 mm, SEM = ± 9.13 mm), again closely matching the vestibular variability trial (mean = 47.82 mm, SEM = ± 5.53 mm). The close match suggests that participants integrated the coherent, real-time component during calibration, and their postural response became dominated by the added non-coherent noise, limiting recovery toward baseline.

In the no-noise condition, the pattern differed across order groups. Group A (mean = 19.13 mm, SEM = ± 2.59 mm) displayed post-calibration variability close to the vestibular variability level (mean = 13.49 mm, SEM = ± 0.82 mm), whereas group B shows substantially higher variability (42.42 mm), likely due to the carryover effect from the preceding noise condition.
Closer inspection of the group B no-noise trials revealed that this elevated mean was driven by two participants who exhibited brief episodes of complete loss of balance. Outside these isolated events, their sway variability aligned with the rest of the group. Without these episodes, the post-calibration variability would fall much closer to the vestibular variability values. This adjusted pattern more closely matches the expected behavior when coherent stimulation is interpretable and aligns with previous findings showing that participants generally adapt to coherent, real-time input (Héroux et al. (2015); Chen et al. (2022)).

3.5. Impact of Order Effects

To examine how stimulation condition and presentation order influenced postural variability, both the absolute standard deviation of T1 displacement and the relative standard deviation (normalised to each participant's baseline) were analysed.

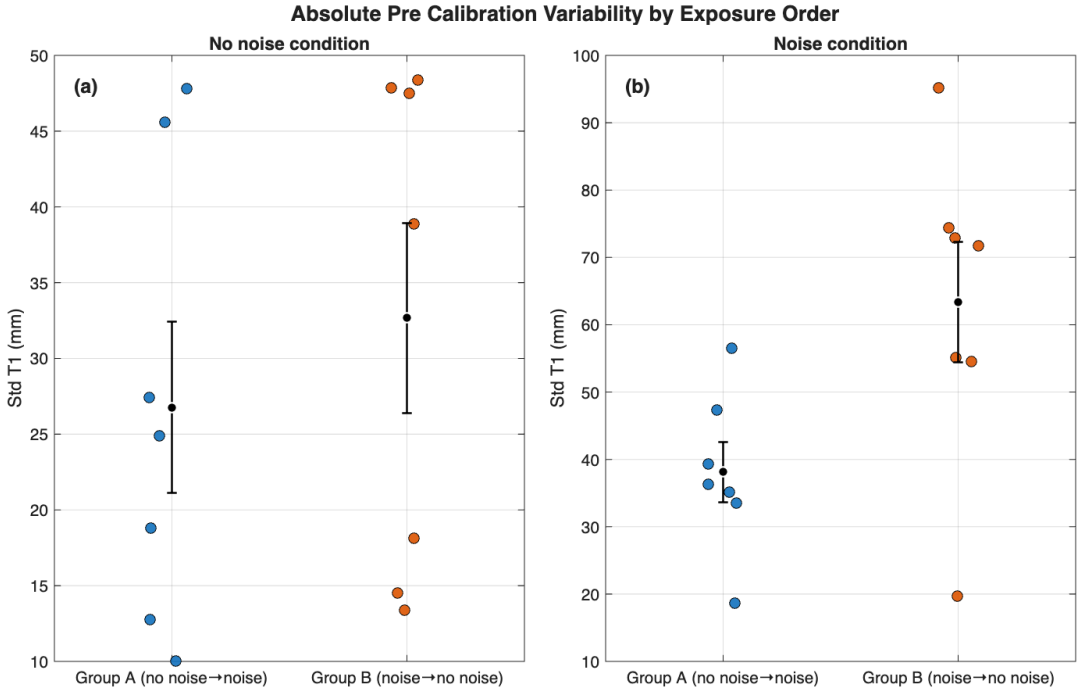

Figure 3.3: Absolute Standard Deviation T1 based on order.
Panel (a) shows the SD of T1 displacement for the no-noise condition, while panel (b) shows the same measure for the noise condition. Each dot represents an individual participant's relative variability. Black markers indicate the group mean, and error bars represent the standard error of the mean.

Absolute Standard Deviation The absolute sternum displacement variability across the no-noise and noise conditions for both order groups is illustrated in Figure 3.3. Variability is consistently higher in the noise condition for most participants, while differences between the two order groups appear comparatively small. A two-way mixed ANOVA with condition as a within-subject factor and order as a between-subject factor reveals a significant main effect of condition ($F(1,12) = 14.511$, $p = 0.002$), indicating reliably greater variability during noise stimulation. Although the main effect of order approached significance ($p = 0.057$), there was no clear evidence that exposure order systematically influenced absolute variability. Additionally, the condition × order interaction was not significant ($F(1,12) = 3.076$, $p = 0.105$), indicating that the influence of stimulation type did not vary meaningfully as a function of whether the noise condition was experienced first or second. Overall, the absolute variability results show that noisy vestibular stimulation increases postural variability, but the presentation order does not significantly modify this effect.

Relative Standard Deviation To account for individual differences in baseline stability, variability was additionally expressed relative to each participant's baseline standard deviation (Figure 3.4). Once normalised, the differences between conditions and order groups appeared reduced compared to the absolute values. A mixed ANOVA on the relative variability revealed no significant main effect of condition, ($F(1,12) = 4.105$, $p = 0.066$), and no significant main effect of order ($F(1,12) = 0.604$, $p = 0.452$). The condition × order interaction was likewise not significant ($F(1,12) = 2.869$, $p = 0.116$). These results indicated that when baseline sway is taken into account, neither the stimulation type nor the order of presentation produces reliable differences in relative sternum variability.

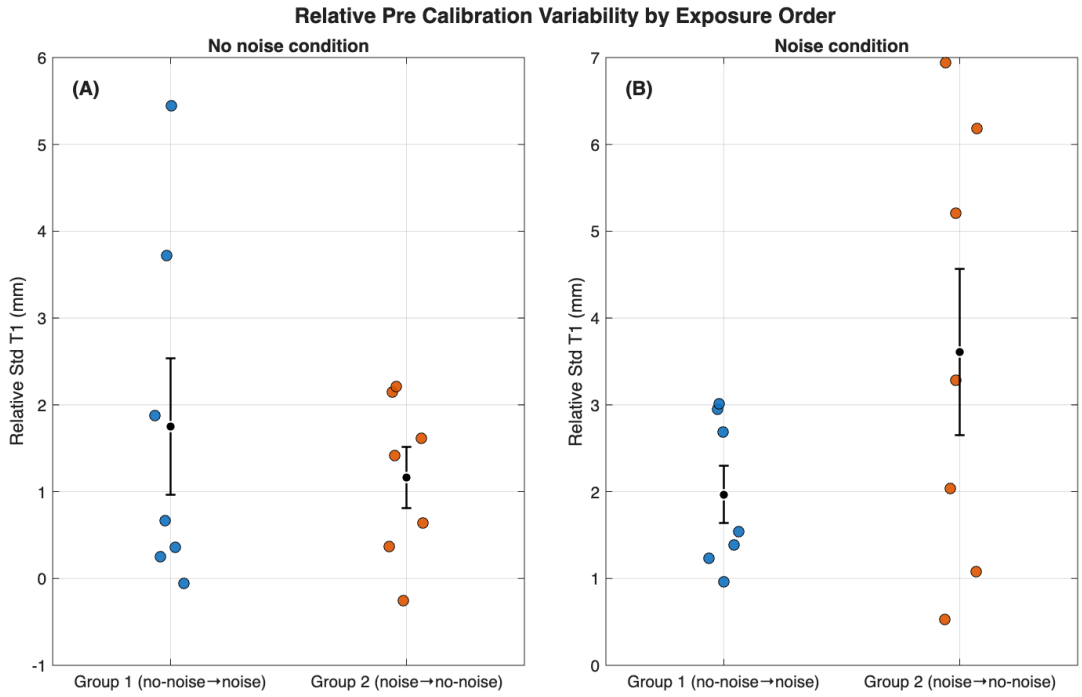

Figure 3.4: Relative Standard Deviation T1 based on order.
Panel (a) shows the relative SD of T1 displacement for the no-noise condition, while panel (b) shows the same measure for the noise condition. Each dot represents an individual participant's relative variability, normalized to their baseline standard deviation to account for individual differences in natural stability. Black markers indicate the group mean, and error bars represent the standard error of the mean (SEM).

3.6. Influence of Natural Postural Stability on Adaptive Learning

To evaluate whether participants' natural postural stability influences their ability to learn during the vestibular recalibration experiment, the relationship between learning and the baseline standard deviation of T1 displacement in the Y-axis is examined (Figure 3.5). This baseline variability reflects each participant's natural sway during quiet standing with eyes closed and no stimulation. If greater baseline variability (i.e., poorer natural balance) facilitates adaptation, a positive linear relationship between baseline SD and learning is expected. However, Pearson correlation analyses revealed no significant association between natural baseline variability and learning in either condition. In the no-noise condition, the correlation was r = 0.39 (p = 0.39), whereas in the noise condition it was r = –0.32 (p = 0.48). Consistent with these statistics, the scatter plots for both the no-noise (left) and noise (right) conditions show no systematic trend; participants with either higher or lower baseline sway exhibited similar learning outcomes. Thus, baseline sway does not predict adaptation performance. Although baseline variability is generally higher in the noise condition, reflecting the disruptive effect of non-coherent vestibular input observed in other analyses, this increased variability does not translate into differences in learning.

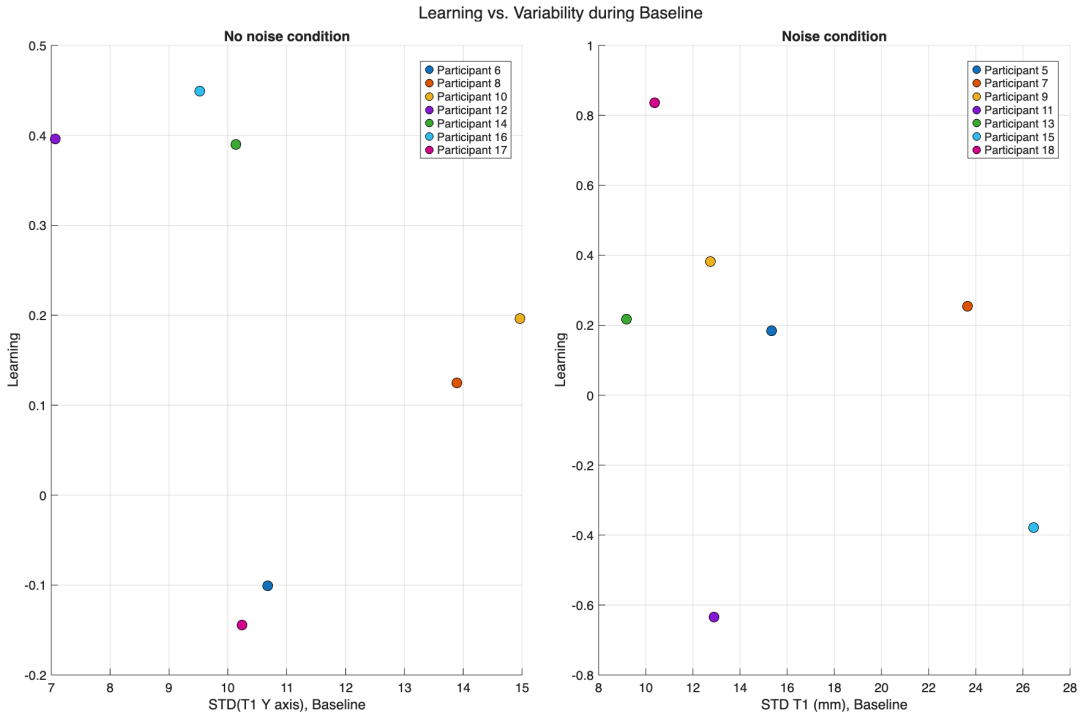

Figure 3.5: Each panel shows individual participants' learning values plotted against their baseline standard deviation of T1 displacement in the Y-axis. The left panel corresponds to the no-noise condition, and the right panel to the noise condition. Each color represents a different participant.

3.7. Stimulation after-effect

To investigate whether an after-effect of vestibular stimulation persists after stimulus cessation, the post-stimulation variability during the recovery segment is compared with each participant's baseline variability. Initial inspection of Figure 3.2 suggests that, across participants, the variability of T1 motion during the recovery segment appears higher than at baseline. This observation is consistent with the possibility that exposure to vestibular stimulation temporarily destabilizes balance beyond the duration of the stimulus. A comparable after-effect has been documented by Héroux et al. (2015), who reported that balance becomes more unstable than baseline following adaptation to vestibular input. However, because averaging across the entire recovery segment could obscure short-lived responses (e.g., an initial transient elevation that rapidly returns to baseline), the sliding standard deviation of T1 motion was used to examine temporal evolution during the full 40-s period without stimulation.

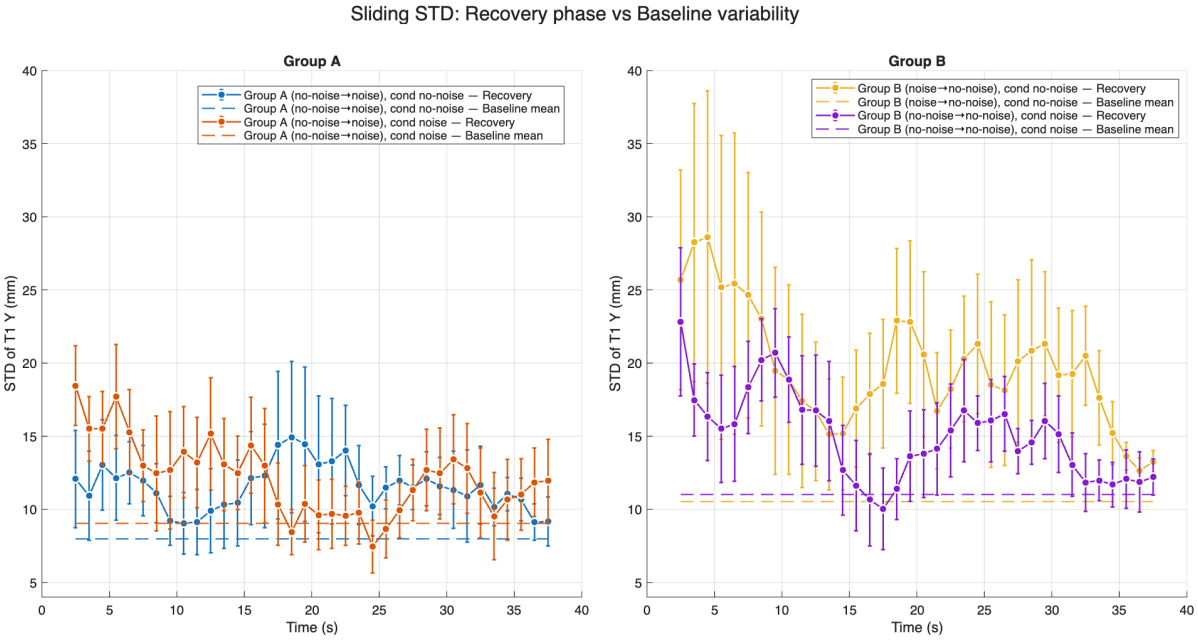

Figure 3.6: Comparison of sliding STD during recovery (solid) and baseline (dashed). Solid lines show recovery sliding-window variability, while dashed lines show corresponding baseline values for each group and condition. In group B under condition 4, variability remains elevated throughout most of the sequence, supporting the presence of a sustained after-effect. Other groups show smaller increases above baseline, suggesting limited or weaker persistence of the stimulation effect.

For participants who experienced the no-noise condition first (Group A), a paired t-test showed that post-stimulation variability was significantly higher than baseline (baseline: 10.94 ± 3.17 mm; recovery: 18.74 ± 10.45 mm; $p = 0.0088$). Although significant, this after-effect was small in magnitude, and its functional relevance remains uncertain.

The noise before no-noise (group B) participants exhibited consistently elevated variability (15.97 ± 4.99 mm;, $p = 0.0011$) throughout most of the recovery period, only approaching baseline levels (12.08 ± 4.19 mm) in the final seconds. These results confirm that postural instability remained elevated for at least 40 s after cessation of vestibular stimulation. As shown in Figure 3.6, both groups displayed a decay in sliding standard deviation values: variability is highest in the first seconds following stimulus offset and then steadily diminishes across the 40-s recovery interval, approaching—but not fully reaching—baseline levels by the end of the trial.

When comparing the magnitude of the after-effect across conditions, the mean after effect sway across the entire period tended to be larger following the no-noise condition (7.81 mm) than the noise condition

(3.89 mm), but this difference is not statistically significant ($p = 0.12$). Likewise, participants in group B exhibited higher average after-effect sway than those in group A, although this group difference does not reach significance ($p = 0.24$). The order × condition interaction, assessed via the difference in after-effect sway between conditions for each subject, also failed to reach significance ($p = 0.21$). Together, these analyses indicate a robust destabilizing after-effect of vestibular stimulation in both conditions, with only suggestive but not statistically reliable modulation by stimulation order.

4

Discussion

This study examined whether the human vestibular system recalibrates when the natural mapping between head motion and vestibular afference is disrupted by non-coherent noise. Previous work has shown that recalibration depends critically on the presence of a stable and interpretable relationship between vestibular input and self-generated movement Héroux et al. (2015). The present findings extend this by demonstrating that short-term recalibration is preserved under both coherent and non-coherent stimulation. These results are interpreted in the context of established models of multisensory reweighting (Peterka (2002); Ernst and Bülthoff (2004)), classical vestibular physiology and internal-model concepts (Highstein et al. (1987); Carver et al. (2006)). Together, these frameworks explain how the CNS differentiates vestibular signals that can support recalibration from those that are unpredictable and therefore resistant to adaptation.

4.1. Recalibration Under Coherent Stimulation

Participants exposed to coherent, motion-linked stimulation demonstrated behavioral evidence of vestibular recalibration. Although the magnitude of improvement varied across individuals, the overall reduction in sway during the calibration phase indicates that participants were able to reinterpret the altered vestibular input when it remained predictably tied to their own head motion. This finding is broadly consistent with Héroux et al. (2015), who showed that humans can adapt to real-time, motion-coupled galvanic vestibular stimulation. In the present study, visual information was available during the calibration phase, providing a stable reference frame that likely facilitated this adjustment. The critical factor, consistent across both datasets, is the preservation of coherent sensorimotor structure. When the vestibular signal maintains a predictable relationship with self-generated motion, the nervous system can treat the manipulated input as a modified, yet still interpretable consequence of movement. Within multisensory weighting frameworks (Peterka (2002)), this corresponds to the CNS maintaining vestibular weighting when the information remains precise, reliable, and internally predictable. While the magnitude of adaptation observed here was smaller and statistically weaker than previously reported, the direction of the effect and its consistency across participants align with expected physiological behavior. Together, these results reinforce the idea that coherent vestibular stimulation supports short-term recalibration through preserved predictability and cross-modal cue alignment.

4.2. Limited Recalibration Under Non-Coherent Noise

Participants in our study showed partial recalibration to the coherent vestibular perturbation: after calibration, sway variability returned to levels comparable to those observed in the vestibular-variability (non-coherent) trials. This pattern suggests that the coherent component was incorporated into the internal model of self-motion, rather than being down-weighted as would be predicted by classical sensory reweighting theory (fPeterka (2002); Carver et al. (2006)). Under that framework, a noisy or unreliable

vestibular signal should be suppressed, preventing recalibration. However, because some adaptation still occurred despite the added noise, our findings do not fully align with a simple down-regulation of vestibular input, consistent with the conclusions of Héroux et al. (2015).

A plausible explanation for the persistence of recalibration under noisy stimulation is that adaptive processes may operate within vestibular pathways that are partially distinct from those supporting real-time balance. Evidence from the vestibulo-ocular reflex (VOR) suggests a dual-pathway organization, with a cerebellum-dependent "modified" pathway capable of adaptation and a more direct "unmodified" pathway that provides rapid, high-fidelity vestibular processing (Ramachandran et al. (2006)). Although this report's experiment did not directly test this architecture, such a division could help explain why participants showed signs of recalibration even when non-coherent noise increased overall sway variability. If adaptive changes were driven primarily by the modified, cerebellar pathway, while real-time balance relied more heavily on the unmodified pathway, then noise in the afferent input would not necessarily disrupt recalibration. As long as the coherent component preserves a consistent relation to head motion, the modified pathway can compute prediction errors and update the internal model, while the unmodified pathway continues to support stable balance control. Thus, our findings are more consistent with a parallel-pathway processing scheme (Ramachandran et al. (2006)) than with a sensory reweighting mechanism. This framework remains speculative in the context of our data but provides a mechanistic hypothesis that could be tested directly in future work.

Additional evidence for such a multi-pathway organization comes from both peripheral and central vestibular physiology. Highstein et al. (1987) showed that secondary vestibular neurons projecting to oculomotor, spinal, and cerebellar targets receive different mixtures of regular and irregular afferent inputs, demonstrating an early anatomical divergence into functionally distinct central channels. Ramachandran et al. (2006) extended this framework within the VOR, identifying a cerebellum-dependent modified pathway and a direct unmodified pathway, and showing that this division cannot be explained solely by afferent regularity. This aligns with Highstein et al. (1987), who found that central vestibular neurons integrate diverse afferent types. Together, these studies indicate that vestibular processing involves multiple layers of specialization—peripheral (regular vs. irregular) and central (modified vs. unmodified). This forms a hierarchical set of parallel computational pathways.

A further line of evidence supporting a multi-pathway vestibular architecture comes from the differential coding strategies identified by Mackrous et al. (2020). They showed that central vestibular neurons differ in how variable their firing is: low-variability neurons, mainly those involved in the VOR, closely track the actual motion signal, while high-variability neurons perform temporal whitening, reducing correlations in the incoming motion signal to produce a more uniform and efficient representation (Mackrous et al. (2020)). This functional split aligns with the idea of 'unmodified' and 'modified' pathways: the unmodified pathway supports fast, stable motor control, while the modified pathway is better suited for updating internal estimates based on prediction errors. Notably, Mitchell et al. (2018) showed that whitening emerges centrally and cannot be explained by afferent properties alone, reinforcing the view that central vestibular processing comprises parallel computational channels optimized for distinct roles. This framework provides a mechanistic basis for our finding that recalibration persists despite added non-coherent noise: adaptive updating can proceed within the whitening-associated pathway even as real-time balance control relies on the high-fidelity channel.

4.3. Order-Dependent Effects

Despite the absence of statistically significant effects, the descriptive patterns shown in Figure 3.4 suggest potential order-related influences on pre-conditioning variability. In the noise condition (Figure 3.4B), participants in group B showed higher and more widely dispersed relative variability values (approximately 0.5–7mm) compared to those in group A, whose values were more narrowly distributed (around 0.9–3mm). This pattern suggests that participants exposed to noise later in the protocol may

have been less destabilised by the noisy stimulus. A weaker version of this pattern is visible in the no-noise condition (Figure 3.4A), where variability tended to be lower when the no-noise condition occured second, consistent with a possible after-effect from prior noise exposure. Although these descriptive differences do not reach statistical significance, they may point to order-related influences on variability, particularly during the noise condition, that are not fully captured in the inferential tests.

A plausible interpretation is that early exposure to highly unreliable vestibular cues shifts sensory weighting more aggressively away from the vestibular modality. Once down-weighted, the system may be slow to reinstate vestibular reliability, consistent with the persistence of recalibrated sensory weights observed by Héroux et al. (2015) and Carver et al. (2006) and the established reliability-weighting frameworks by Peterka (2002). The work by Carver et al. (2006) demonstrated that when a sensory modality becomes unreliable the nervous system rapidly down-weights that modality, whereas the subsequent up-weighting once reliability is restored occurs much more slowly. This temporal asymmetry reflects a form of short-term sensory "memory," in which early exposure to unreliable cues leads to a lingering reduction in sensory weight. Our results are consistent with this framework: participants who experienced high-amplitude vestibular noise first appeared less destabilized by subsequent noise exposure, suggesting that the vestibular modality had already been down-weighted and was slow to regain its original weighting once coherent input reappeared. Because our calibration phase relied on visual information to recalibrate the vestibular signal, the parallels to visual adaptation are especially relevant—both systems exhibit rapid suppression in response to unreliable input, followed by slow recovery. This correspondence strengthens the interpretation that short-term sensory history meaningfully shapes the rate, though not necessarily the final extent, of vestibular recalibration in our paradigm.

4.4. Natural Stability Effects

No relationship is observed between baseline sway and learning in either condition. This indicates that natural balance ability does not determine an individual's capacity for vestibular recalibration within this protocol. Instead, adaptation appears governed primarily by the reliability and coherence of the afferent signal, consistent with sensory-integration theory (Peterka (2002)). This result reinforces the interpretation that recalibration reflects central processing constraints rather than peripheral or biomechanical stability differences.

The heightened inter-individual differences observed in the experiments align closely with the findings of Goodworth et al. (2023), who showed that variability in postural responses arises primarily from differences in central sensorimotor feedback parameters, including vestibular weighting, integral gain, and neural time delay. In particular, Goodworth et al. (2023) report that sensory weighting and integral gain display the largest natural variability across individuals, and these parameters strongly predict differences in the average sway amplitude under perturbation. This framework provides a mechanistic explanation for why some participants in the present experiment adapted effectively even under added noise, while others remained dominated by the perturbation. Consistent with the findings of Goodworth et al. (2023), that challenging stimuli amplify inter-subject differences, the high-noise condition in our experiment similarly revealed pronounced divergence in participants' ability to extract and recalibrate the coherent component of the stimulus.

4.5. Post-Stimulation After-Effects

Across both conditions, sway remained elevated after the stimulus was turned off, indicating short-term after-effects of vestibular perturbation. These after-effects were particularly pronounced when noise was experienced first, suggesting that the CNS requires additional time to restore the pre-exposure sensory integration. Similar after-effects were observed by Héroux et al. (2015), who attributed them to short-term recalibration of the brain's internal expectations rather than to any lingering biomechanical effect. The present findings support this view: the lingering instability likely reflects delayed re-

establishment of the original vestibular weighting after temporary adaptation to degraded or inconsistent cues.

4.6. Future work

Several avenues for future research emerge from the present findings and their limitations. First, post-stimulation recordings should be extended beyond the 40-s recovery period. The elevated sway observed in some participants suggests that after-effects may evolve over longer timescales than captured in the current protocol. Extended monitoring would enable characterization of full recovery dynamics and determination of whether post-exposure destabilization decays rapidly, plateaus, or undergoes secondary adjustments. Second, the conversion model and stimulation mapping used in this work may interact with individual differences in vestibular sensitivity. Incorporating subject-specific calibration—either through personalized gain tuning or individualized transfer-function weighting—may reduce inter-participant variability and better isolate true differences in adaptive capability. Such approaches would also allow testing whether individuals with higher vestibular gain or lower sensory noise exhibit more robust recalibration. Third, future studies should investigate whether prolonged training or repeated exposure sessions enable adaptation under conditions that initially appear resistant to recalibration. If the disruptive effect of non-coherent noise is primarily short-term, extended training may allow the CNS to extract stable structure from the stimulus over time.

A related question involves systematically varying the degree of noise coherence. Instead of a binary noise/no-noise design, introducing partially coherent stimuli would allow testing whether learning degrades in a graded manner as the motion–afference mapping becomes increasingly unreliable. This would directly quantify the threshold at which noise prevents recalibration. Additionally, examining larger noise amplitudes may reveal nonlinear effects or floor limits in learning that were not detectable within the current stimulation range. Together, these directions would provide a more detailed understanding of how the CNS interprets altered vestibular signals, the limits of recalibration under degraded conditions, and the role of multisensory information in restoring postural stability.

5

Conclusion

This report set out to answer the question: Is the nervous system able to recalibrate its expectation of motion when the inherent motion-to-sensation relation is compromised by noise? The results showed that recalibration is indeed possible when the vestibular input maintains a coherent link to head motion. However, when this relationship is disrupted by noise, the ability to adapt becomes noticeably limited.

More broadly, these findings highlight the importance of coherent sensory cues for maintaining balance and for updating our internal sense of motion. They also suggest that when these cues become unreliable—whether through noise, injury, or artificial stimulation—the nervous system's ability to adapt may be reduced, but not entirely lost.
Insights from this work can help guide the design of future vestibular stimulation tools, rehabilitation strategies, and assistive technologies that rely on artificially manipulating balance-related signals. By knowing how the brain responds to different types of altered vestibular input, future systems can be designed to support adaptation rather than disrupt it. In this way, the findings contribute to a growing foundation of knowledge that can improve clinical, experimental, and technological approaches to balance and vestibular function.

References

Héroux, Martin E. et al. (Apr. (2015)). “Cross-Modal Calibration of Vestibular Afference for Human Balance”. In: *PLOS ONE* 10.4. Accessed 7 Apr. 2023, e0124532. DOI: 10.1371/journal.pone.0124532. URL: https://doi.org/10.1371/journal.pone.0124532.

Chen et al. (Feb. (2020)). “Development of a Conversion Model between Mechanical and Electrical Vestibular Stimuli”. In: *Journal of Neurophysiology* 123.2, pp. 548–559. DOI: 10.1152/jn.00276.2019. URL: https://doi.org/10.1152/jn.00276.2019.

Shadmehr et al. ((2008)). “A computational neuroanatomy for motor control”. In: *Experimental Brain Research* 185.3, pp. 359–381. DOI: 10.1007/s00221-008-1280-5. URL: https://doi.org/10.1007/s00221-008-1280-5.

Carriot et al. ((2015)). “Rapid Adaptation of Multisensory Integration in Vestibular Pathways”. In: *Frontiers in Systems Neuroscience* 9, p. 59. DOI: 10.3389/fnsys.2015.00059. URL: https://doi.org/10.3389/fnsys.2015.00059.

Fitzpatrick, Richard C. and Brian L. Day (June (2004)). “Probing the Human Vestibular System with Galvanic Stimulation”. In: *Journal of Applied Physiology* 96.6, pp. 2301–2316. DOI: 10.1152/japplphysiol.00008.2004. URL: https://doi.org/10.1152/japplphysiol.00008.2004.

Maurer et al. (Nov. (2005)). “Multisensory Control of Human Upright Stance”. In: *Experimental Brain Research* 171.2. Accessed 8 Apr. 2021, pp. 231–250. DOI: 10.1007/s00221-005-0256-y. URL: https://doi.org/10.1007/s00221-005-0256-y.

Chen et al. (Dec. (2022)). “A Portable and Low-Cost Solution for Real-Time Manipulation of the Vestibular Sense”. In: *Journal of Neuroscience Methods* 382. Accessed 13 Feb. 2023, p. 109709. DOI: 10.1016/j.jneumeth.2022.109709. URL: https://doi.org/10.1016/j.jneumeth.2022.109709.

Schneider, Adam D. et al. (Apr. (2015)). “The Increased Sensitivity of Irregular Peripheral Canal and Otolith Vestibular Afferents Optimizes Their Encoding of Natural Stimuli”. In: *The Journal of Neuroscience* 35.14. Accessed 15 Sept. 2023, pp. 5522–5536. DOI: 10.1523/jneurosci.3841-14.2015. URL: https://doi.org/10.1523/jneurosci.3841-14.2015.

Kwan, Annie et al. (Apr. (2019)). “Neural Substrates, Dynamics and Thresholds of Galvanic Vestibular Stimulation in the Behaving Primate”. In: *Nature Communications* 10.1. DOI: 10.1038/s41467-019-09738-1. URL: https://doi.org/10.1038/s41467-019-09738-1.

Khosravi Hashemi, Navid et al. (Sept. (2019)). “Virtual Signals of Head Rotation Induce Gravity□Dependent Inferences of Linear Acceleration”. In: *The Journal of Physiology* 597.21. Accessed 4 July 2025, pp. 5231–5246. DOI: 10.1113/JP278642. URL: https://doi.org/10.1113/jp278642.

Wu, Lyndia C. et al. (Aug. (2015)). “In Vivo Evaluation of Wearable Head Impact Sensors”. In: *Annals of Biomedical Engineering* 44.4, pp. 1234–1245. DOI: 10.1007/s10439-015-1423-3. URL: https://doi.org/10.1007/s10439-015-1423-3.

Peterka, Robert J. (Sept. (2002)). “Sensorimotor Integration in Human Postural Control”. In: *Journal of Neurophysiology* 88.3, pp. 1097–1118. DOI: 10.1152/jn.2002.88.3.1097. URL: https://doi.org/10.1152/jn.2002.88.3.1097.

Ernst, Marc O. and Heinrich H. Bülthoff ((2004)). “Merging the senses into a robust percept”. In: *Trends in Cognitive Sciences* 8.4, pp. 162–169. DOI: 10.1016/j.tics.2004.02.002.

Highstein et al. ((1987)). “Inputs from regularly and irregularly discharging vestibular-nerve afferents to secondary neurons in the vestibular nuclei of the squirrel monkey. II. Correlation with output pathways of secondary neurons”. In: *Journal of Neurophysiology* 58, pp. 719–738.

Carver et al. ((2006)). “Modeling the dynamics of sensory reweighting”. In: *Biological Cybernetics* 95.2, pp. 123–134. DOI: 10.1007/s00422-006-0069-5.

Ramachandran et al. (Sept. (2006)). “Transformation of Vestibular Signals into Motor Commands in the Vestibuloocular Reflex Pathways of Monkeys”. In: *Journal of Neurophysiology* 96.3, pp. 1061–1074. DOI: 10.1152/jn.00281.2006. URL: https://doi.org/10.1152/jn.00281.2006.

Mackrous, Isabelle et al. ((2020)). “Neural variability determines coding strategies for natural self-motion in macaque monkeys”. In: *eLife* 9. Published September 11, 2020. Accessed 10 Nov. 2025. DOI: 10.7554/eLife.57484. URL: https://doi.org/10.7554/eLife.57484.

Mitchell et al. ((2018)). “Neuronal Variability and Tuning Are Balanced to Optimize Naturalistic Self-Motion Coding in Primate Vestibular Pathways”. In: *eLife* 7. Accessed 10 Nov. 2025. DOI: 10.7554/eLife.43019. URL: https://doi.org/10.7554/eLife.43019.

Goodworth et al. ((2023)). “Variation between individuals in sensorimotor feedback control of standing balance”. In: *Journal of Neurophysiology* 130.4, pp. 303–318. DOI: 10.1152/jn.00353.2022.